A Combined Method-of-Moments and Near-Field Measurements for EMI Evaluation of Switched-Mode Power Supplies

Sayyed Mohammad Mehdi Mirtalaei, Seyed Hossein H. Sadeghi, *Senior Member, IEEE*, and Ruzbeh Moini, *Senior Member, IEEE*

***Abstract*—We propose an efficient modeling technique for the evaluation of radiated electromagnetic interference due to a switch-mode power supply mounted on a typical electronic printed circuit board (PCB). In the proposed model, first, the measured magnetic field on a rectangular plane in the vicinity of the PCB is used to identify equivalent current sources on the board surface by the method-of-moments. Having determined the radiating sources, the governing integral equations in free space are then utilized to compute the magnetic-field distribution at a desired distance from the PCB. The main feature of the proposed model is the use of both the magnitude and phase of the near-magnetic field for identifying the unknown current sources. This is found to be advantageous over the conventional models where the measurements are done on two separate planes or involve time-consuming heuristic optimization algorithms to invert the measured magnetic-field data into unknown current sources. The validity of the proposed technique is demonstrated by comparing the actual and reconstructed field radiations due to several simulated and fabricated sources.**

***Index Terms*—Magnetic-field measurement, method-of-moments, radiation monitoring, switched-mode power supplies (SMPSs).**

I. Introduction

SWITCHED-MODE power supplies (SMPSs) have become very popular in the recent years because of their low cost and size and performance advantages. Developments in the production of high-power and high-frequency semiconductors make it possible to have higher switching frequencies which, in turn, cause weight and volume reduction of SMPSs. However, because of high di/dt currents and high dv/dt voltages in the circuits, they generate conducted and radiated electromagnetic interference (EMI). Hence, electromagnetic compatibility (EMC) is one of the basic issues in the design of SMPSs. As a common practice, SMPS manufacturers use a set of established rules to control various electromagnetic parameters in the design stage [1]–[4], but the final product should be tested according to the EMC standards in a semi-anechoic chamber or in an open-area test site. If the respective EMC tests fail, the manufacturers must modify their designs and repeat the tests. This process is very time consuming and expensive, and hence, more efficient methods are sought to predict radiated emissions from SMPSs in early design stages.

Although many studies have been done on the modeling of conducted EMI, there is limited data on radiated EMI. Three approaches have been proposed for the modeling of radiated EMI. The first approach is based on a simplified analytical model for the radiating components of SMPSs. In this model, the transmission line theory is used for computing the electromagnetic-field radiations in the low-frequency range of below 10–15 MHz. The model is not appropriate in the high-frequency range due to the increasing parasitic couplings and resultant common-mode currents. In the high-frequency range (i.e., above 15 MHz), a number of electrical dipoles have been used to model radiations [5]. Despite its simplicity, this approach provides crude approximations of radiated emissions.

The second approach is based on the use of numerical methods. In [6], a 3-D finite-element model has been proposed to solve the governing equations, with the source current/voltage extracted by measurement or standard circuit analysis. In [7], the finite-difference time-domain method is adopted to examine the electromagnetic resonant effects of various types of heat sinks which are commonly used in SMPSs. The identification of current and voltage sources as well as the modeling SMPS components in this approach is relatively complicated and cumbersome, making it unattractive for treating a complex SMPS.

The third approach is based on the reconstruction of radiating sources [8]–[11]. This approach is used to determine far-field radiations using the respective near-field measurements. It can be summarized in three distinct stages. First, field data are measured on a plane in the vicinity of the printed circuit board (PCB) containing SMPS components. The measured data are then used to identify a set of equivalent radiating sources that generate the same field data as the original ones. Finally, the field value at any point outside the PCB is computed by adding the contributions from all the equivalent sources. Several methods have been proposed for modeling equivalent sources. In [8], the radiating sources on the PCB are modeled as equivalent surface currents whose distribution is obtained using a direct optimization approach. In this technique, which is widely used in antenna characterizations [12]–[16], first, the magnitudes of tangential magnetic field are measured on two

Manuscript received January 13, 2013; revised May 15, 2013; accepted May 24, 2013. Date of publication June 11, 2013; date of current version September 19, 2013.

The authors are with the Department of Electrical Engineering, Amirkabir University of Technology, Tehran 15914, Iran (e-mail: mirtalaei@aut.ac.ir; sadeghi@aut.ac.ir; moini@aut.ac.ir).

Color versions of one or more of the figures in this paper are available online at http://ieeexplore.ieee.org.

Digital Object Identifier 10.1109/TIE.2013.2267703

separate planes in the vicinity of the PCB. The measured data are then used to obtain the unknown equivalent current sources. In this approach, only the magnitude of measurement data is being used. The phase measurement data can be obtained by the phase-retrieval method. While the phase information is easily retrieved in high frequencies, it is not accurately obtained in the low-frequency range that constitutes most of the radiated energy spectrum of SMPSs. This stems from the fact that the separation distance between the two measurement planes is not comparable with the respective wavelengths, thus leading to negligible phase change. Another work modeled the near-field magnetic field of SMPSs by a set of electric and magnetic dipoles [10]. In this approach, pairs of electric and magnetic dipoles have been used as equivalent sources to produce the same near-field distributions as the original sources. The correct locations and moments of the dipole pairs in this method are obtained using the genetic algorithm. Once the equivalent dipole set is determined, the far-field distributions can be easily computed analytically. Despite the accuracy of this method, it is computationally inefficient due to the time-consuming nature of the heuristic search algorithms. Another work models a switching cell by a circular magnetic dipole whose geometrical characteristics and equivalent current are given from the magnetic field measured in the near field. This approach can model the simple structure and cannot work for complicated sources properly [11].

In this paper, we propose a model-based inverse solution for the determination of the unknown equivalent current sources on the PCB, radiating the same near-field distributions around an SMPS. To this end, we use the method-of-moments to solve the governing integral equation, relating the measured tangential component of magnetic field in the near-field region to appropriate equivalent electric current sources on the surface of the PCB. It is worth noting that the measurements are done only on one plane for both the phase and magnitude of the tangential magnetic field. Also, the closed-form expressions used in the inversion process will remarkably reduce the computation burden as compared with the conventional methods where heuristic inversion methods are employed. Having determined the current source, the electromagnetic emissions in the far-field region in free space are readily computed.

This paper is organized as follows. In Section II, the theory and basic formulation of the proposed method are presented. The validity of the proposed technique is demonstrated in Section III where the actual and predicted far-field magnetic-field radiations are compared using simulation and experimental data.

II. Theory

The geometry of the problem is shown in Fig. 1(a). As shown in this figure, a typical PCB contains an SMPS together with its related components, including current loops, high-frequency transformers and inductors, and heat sinks among other electronic devices located at $z = 0$.

To determine the far-field [$z = h_2$ in Fig. 1(a)] magnetic-field distribution in the problem posed earlier, we adopt the electromagnetic equivalence principle [17]. According to this

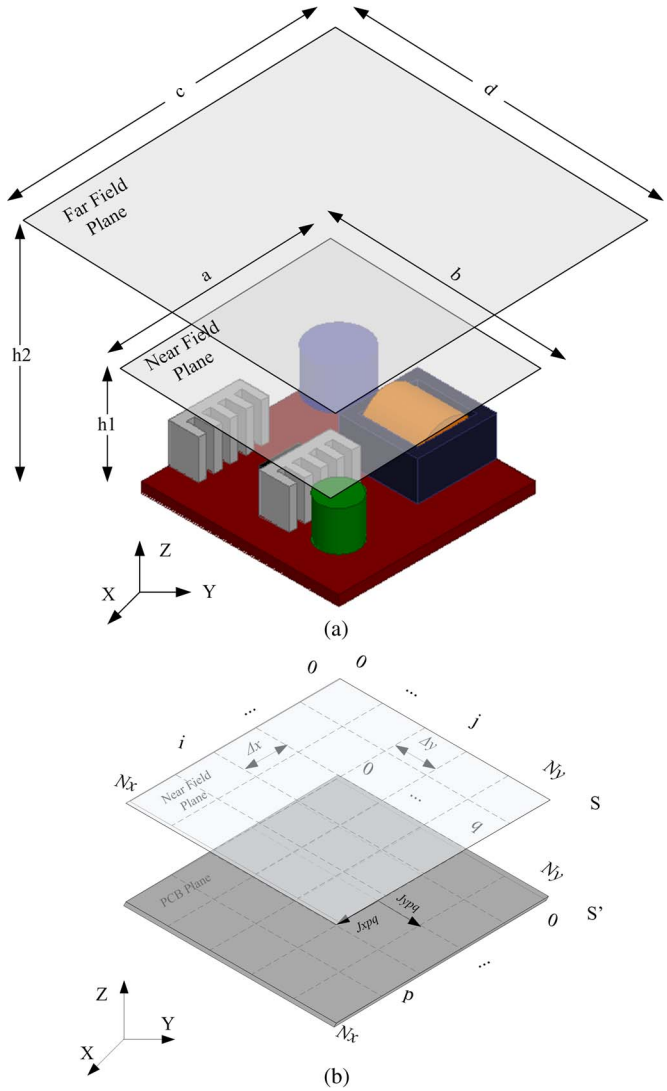

Fig. 1. Geometry of the problem. (a) Original problem composed of an SMPS PCB ($z = 0$) as radiating source, measurement plane in the near-field zone ($z = h_1$), and the far-field plane ($z = h_2$) with unknown magnetic-field distribution. (b) Equivalent problem.

principle, a given set of sources bounded within a closed surface S can be characterized by equivalent electric and magnetic currents distributed on the surface S' that encloses the original sources such that the generated fields outside the surface containing the sources are the same in both the original and the equivalent problem. With reference to Fig. 1(b), the source surface S' is the PCB plane and the bounding surface S is the near-field plane placed at a distance h_1 from the PCB plane. It is assumed that S is large enough to encompass all measurable values of electromagnetic field due to the radiating sources on S'. To determine the equivalent magnetic and electric currents, one needs to know the values of the tangential electric or magnetic-field distributions on the near-field plane S.

The magnetic field $\vec{H}$ in free space due to an arbitrary distribution of electric current J_{eq} is given as follows [18]:

$$\vec{H} = \frac{1}{\mu_0} \nabla \times \vec{A} \tag{1}$$

where μ_0 is the permeability of free space and $\vec{A}$ is the auxiliary magnetic vector potential

$$\vec{A} = \frac{\mu_0}{4\pi} \iint_{S'} \vec{J}_{\text{eq}} \frac{e^{-jkR}}{R}\, ds' \tag{2}$$

and $R = \sqrt{(x-x')^2 + (y-y')^2 + (z-z')^2}$ is the distance between a source point (x', y', z') and an observation point (x, y, z).

By expanding (1) and (2) in the Cartesian coordinates, the values of the magnetic-field component on the near-field plane can be determined as follows:

$$H_x = \frac{1}{4\pi} \iint_{S'} [(z)J_y] \frac{1+jkR}{R^3}\, e^{-jkR} dx'dy' \tag{3}$$

$$H_y = -\frac{1}{4\pi} \iint_{S'} [(z)J_x] \frac{1+jkR}{R^3}\, e^{-jkR} dx'dy' \tag{4}$$

$$H_z = \frac{1}{4\pi} \iint_{S'} [(y-y')J_x - (x-x')J_y] \times \frac{1+jkR}{R_3}\, e^{-jkR} dx'dy' \tag{5}$$

where J_x and J_y represent the x- and y-components of the unknown equivalent electric current density (J_{eq}) on the PCB plane S', respectively.

To solve (3)–(5) for J_x and J_y, we use the method-of-moments [19]. This is done by expanding $\vec{J}_{\text{eq}}$ in terms of the appropriate basis functions in subdomains formed by discrediting S' in N_x and N_y segments along the x- and y-axes, respectively. Using pulse basis function with constant amplitude and phase, we have

$$\vec{J}_{\text{eq}} = \sum_{p=1}^{N_x} \sum_{q=1}^{N_y} (J_{pqx}\hat{x} + J_{pqy}\hat{y}) \prod (x - x_p, y - y_q) \tag{6}$$

where

$$\prod(x,y) = \begin{cases} 1 & |x| < \frac{\Delta x}{2}, |y| < \frac{\Delta y}{2} \\ 0 & |x| > \frac{\Delta x}{2}, |y| > \frac{\Delta y}{2} \end{cases} \tag{7}$$

$$x_p = p\Delta x - \frac{\Delta x}{2} \tag{8}$$

$$y_q = q\Delta y - \frac{\Delta y}{2} \tag{9}$$

and J_{pqx} and J_{pqy} are the unknown coefficients associated with the x- and y-components of J_{eq} on subdomain pq, respectively.

By substituting (6) into (3)–(5) and using the Galerkin method [19], the integral equations relating the magnetic fields to the equivalent electric current density on the PCB are reduced to a system of linear equations as follows:

$$\begin{bmatrix} H_x \\ H_y \\ H_z \end{bmatrix} = \begin{bmatrix} 0 & Z_{H_x,J_y} \\ Z_{H_y,J_x} & 0 \\ Z_{H_z,J_x} & Z_{H_z,J_y} \end{bmatrix} \begin{bmatrix} J_{x\ \text{eq}} \\ J_{y\ \text{eq}} \end{bmatrix} \tag{10}$$

where

$$Z_{H_x,J_y}(ij,pq) = -Z_{H_y,J_x}(ij,pq) = \frac{1}{4\pi}(z)\frac{1+jkR_{ij,pq}}{R_{ij,pq}}\, e^{-jkR_{ij,pq}} \Delta x \Delta y \tag{11}$$

$$Z_{H_Z,J_x}(ij,pq) = \frac{1}{4\pi}(y_{ij} - y_{pq})\frac{1+jkR_{ij,pq}}{R^3_{ij,pq}}\, e^{-jkR_{ij,pq}} \times \Delta x \Delta y \tag{12}$$

$$Z_{H_z,J_y}(ij,pq) = -\frac{1}{4\pi}(x_{ij} - x_{pq})\frac{1+jkR_{ij,pq}}{R^3_{ij,pq}}\, e^{-jkR_{ij,pq}} \times \Delta x \Delta y \tag{13}$$

and $R = \sqrt{(x_i - x'_p)^2 + (y_i - y'_p)^2 + (z_i - z'_p)^2}$.

It is worth noting that there is no singularity in (11)–(13) as $R_{ij,pq}$ always takes a nonzero value. This is due to the fact that the source points (located on the PCB plane) and the observation points (located on plane h_1) never coincide.

From (10), it is found that the unknown values of J_x and J_y can be determined using the measured tangential magnetic field. In fact, the use of tangential magnetic field decouples (10) as follows:

$$[H_{x\ \text{measured}}] = [Z_{H_x,J_y}][J_{y\ \text{eq}}] \tag{14}$$

$$[H_{y\ \text{measured}}] = [Z_{H_x,J_y}][J_{x\ \text{eq}}]. \tag{15}$$

Since Z_{H_x,J_y} and Z_{H_y,J_x} are large and square matrices, the direct inversion methods are generally not efficient for solving (14) and (15). Instead, we use an iterative method such as the least square residual method to treat the problem [20].

Having determined the unknown current sources on the PCB, the radiated far-field magnetic field can be readily obtained using (10).

III. Model Verification and Results

To demonstrate the validity of the proposed model, we first consider two special cases for which analytical solutions are available. These are a small electrical loop (a low-impedance source) and a small electrical dipole (a high-impedance source). The former case represents electrical loops, while the latter simulates the heat sinks on a PCB. We then present the theoretical and experimental results for a more practical case of a typical SMPS. This case serves to show the generality of the model.

The setup shown in Fig. 2 is used to measure the magnetic-field components on the near-field plane ($z = h_1$ in Fig. 1). The setup consists of a Rohde & Schwarz Hz-11 EMI probe set, a 3-D motorized computer-controlled scanner, and a Rohde & Schwarz ZVK-4GHz vector network analyzer (VNA). The scanning time depends on the sampling surface size and mesh density, frequency range, the number of measured field components, and the mechanical speed of the scanner. The sampling surface size should be large enough to cover the majority of the radiated energy, whereas the mesh density is a function of the probe size. The selection of probe size is a tradeoff between the measurement sensitivity and spatial resolution. In addition, smaller probes generally introduce less distortion to

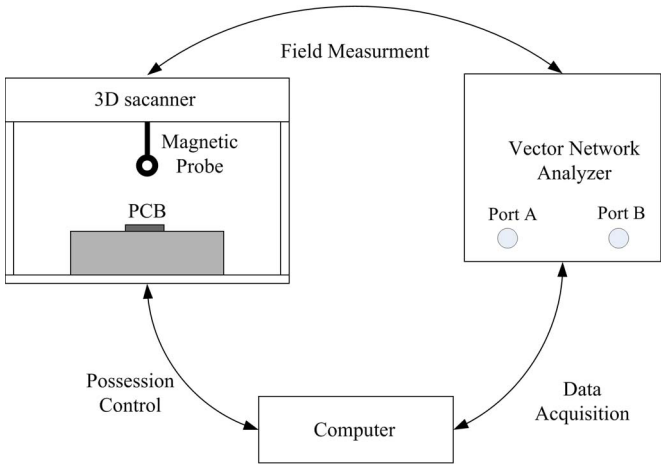

Fig. 2. Experimental setup for magnetic-field measurements.

the measured field. Thus, a smaller probe is preferred for EMI measurement as long as the signal-to-noise ratio (SNR) is large enough at the receiving equipment.

The probe used in this work is an H-field loop probe with 10-mm diameter. The surface sampling size is 140 mm $\times$ 140 mm with a mesh size of 10 mm $\times$ 10 mm. The overall measurement time for obtaining the x- and y-field components is about 25 min. Notice that prior to the measurements, the probe is calibrated by comparing the simulated and measured values of the probe antenna factor associated with a microstrip transmission line [21].

While the measurement of field magnitude radiated from an SMPS is straightforward, its phase measurement is somewhat difficult. This is due to the fact that SMPSs are self-powered devices with no appropriate reference to obtain the phase information. For solving this problem, a dual-probe measurement scheme is used [22]. In this scheme, the VNA operates in its external source mode, allowing it to read the absolute values of signals fed to each receiver and their ratios. As shown in Fig. 2, receiver port A (connected to the measuring probe) moves on the scanning plane and measures the probe voltage V_0 while receiver port B (connected to a stationary reference probe) measures the reference voltage $V_{\rm ref}$. The value of V_0 represents the field magnitude while variations in the phase of $V_0/V_{\rm ref}$ provide the phase information of the field.

A. Small Electrical Loop

In the first case study, we examine the performance of the proposed model when dealing with low-impedance sources. The radiating source is a radiating loop of radius $r = 10$ mm placed at the center of the PCB ($h = 0$ in Fig. 1). The loop is excited with a 1-A sinusoidal current source of frequency $f = 30$ MHz.

Using the well-known field expressions for a radiating loop in free space [18], the variations of the tangential magnetic field (H_x and H_y) are calculated to produce simulated measured data on a near-field plane. Referring to Fig. 1, field calculations are performed on a square plane with ($a = b = 100$ mm) and $N = N_x \times N_y = 2601$ points at an equally spaced $\Delta x = \Delta y = 2$ mm, as shown in Fig. 3.

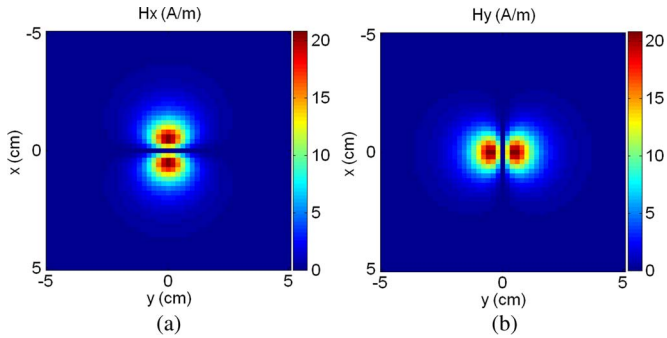

Fig. 3. Variations of the tangential magnetic field on a near-field plane ($h_1 = 10$ mm) produced by an electrical loop of radius 10 mm at the center of the PCB plane (Fig. 1) when excited with a 1-A sinusoidal current source of frequency $f = 30$ MHz. (a) H_x and (b) H_y.

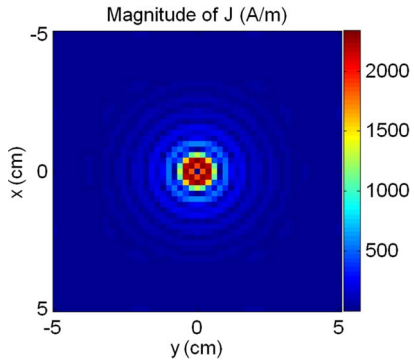

Fig. 4. Variations of the predicted current ($J_{\rm eq}$) on the PCB plane (Fig. 1) using the magnetic-field data shown in Fig. 3.

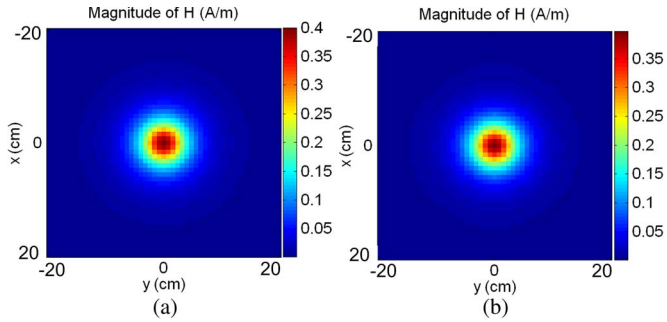

Fig. 5. Variations of the magnitude of magnetic field on a far-field plane ($h_2 = 50$ mm), produced by an electrical loop of radius 10 mm at the center of the PCB plane (Fig. 1) when excited with a 1-A sinusoidal current source of frequency $f = 30$ MHz. (a) Theoretical and (b) reconstructed data.

To show the effect of measurement noise on the simulated data, the values of H_x and H_y on the near-field plane are superposed by Gaussian noise with various values of SNR. The noisy data are then used as input measurement entries to the proposed model, producing equivalent electrical current distribution on the PCB. Results are shown in Fig. 4 for $SNR = 30$ dB. The equivalent current distribution is finally used to compute the field distribution on a far-field plane ($h_2 = 50$ mm and $c = d = 400$ mm).

A visual comparison of the actual and reconstructed results shown in Fig. 5 demonstrates the suitability of the proposed model. For the quantitative assessment of the model validity, we use the feature selective validation (FSV) method. The

TABLE I
VALUES OF ADM, FDM, GDM, AND GRADE–SPREAD FOR ACTUAL AND RECONSTRUCTED RESULTS SHOWN IN FIG. 5

	ADM	FDM	GDM
Value	Excellent (0.030)	Excellent (0.026)	Excellent (0.047)
Grade/Spread	1/1	1/1	1/1

TABLE II
VALUES OF GDM AND GRADE–SPREAD FOR ACTUAL AND RECONSTRUCTED FAR-FIELD DATA WHEN GAUSSIAN NOISE OF VARIOUS SNRS IS SUPERIMPOSED TO SIMULATED FIELD DATA

SNR (dB)	30	20	10	0
GDM	Excellent (0.047)	Very Good (0.107)	Good (0.388)	Very Poor (1.614)
Grade/Spread	1/1	2/2	4/4	6/4

FSV method was first introduced in [23] and [24] and then represented as an IEEE standard [25]. It allows an objective quantified comparison of data for the inter-alia validation of computational electromagnetics. This is done by decomposing each data set into two component measures, namely, amplitude difference measure (ADM) and feature difference measure (FDM). The former compares the amplitudes and trends of the data sets while the latter compares their rapidly changing features. ADM and FDM will then be used to calculate the global difference measure (GDM), which is a global goodness of fit measure. ADM, FDM, and GDM are presented numerically or with a natural language descriptor, namely, less than 0.1: excellent, between 0.1 and 0.2: very good, between 0.2 and 0.4: good, between 0.4 and 0.8: fair, between 0.8 and 1.6: poor, and greater than 1.6: very poor. The FSV method provides another figure of merits called Grade–Spread. Grade gives a numerical indication of the quality of the comparison while Spread represents a numerical indication of the level of confidence that can be placed on the assessment. Grade and Spread can take integer numbers from 1 to 6, being interpreted in a reversed fashion, i.e., 1 corresponds to the highest quality and 6 relates to the lowest quality of comparison.

A quantitative comparison of the actual and reconstructed data shown in Fig. 5 can be found in Table I. The results in this table clearly confirm the validity of the proposed reconstruction model. To study the effect of measurement noise on the reconstruction accuracy, we have repeated the reconstruction process for various values of SNR. The respective values of GDM and Grade–Spread are given in Table II. As can be seen in this table, the validity of the proposed model tends to fail as SNR decreases.

To study the effect of sampling distance (Δx and Δy in Fig. 1) on the accuracy of the proposed technique, we have used several simulated field data on the measurement plane (i.e., $z = h_1$ in Fig. 1) with various degrees of coarseness. For the sake of comparison, we assume $SNR = 30$ dB which is unchanged in all cases. A quantitative comparison between the actual and reconstructed field distributions on a far-field plane ($h_2 = 50$ mm and $c = d = 400$ mm) can be found in Table III. From the results illustrated in this table, it is revealed that the proposed technique is readily converged for a wide range of sampling distances on the field measurement plane. However, the number of measurement data should be large enough (i.e., larger computation time) to achieve accurate results.

TABLE III
VALUES OF GDM, GRADE–SPREAD, AND COMPUTATION TIME FOR ACTUAL AND RECONSTRUCTED FAR-FIELD DATA WHEN SAMPLING SURFACE MESH DENSITIES ($\Delta x = \Delta y$) OF VARIOUS SIZES ARE USED FOR COMPUTING SIMULATED FIELD DATA

$\Delta x = \Delta y$ (mm)	2	5	10	20
GDM	Excellent (0.047)	Fair (0.447)	Fair (0.470)	Poor (0.815)
Grade/Spread	1/1	5/5	5/5	5/5
Run Time (s)	390	3.59	0.23	0.11

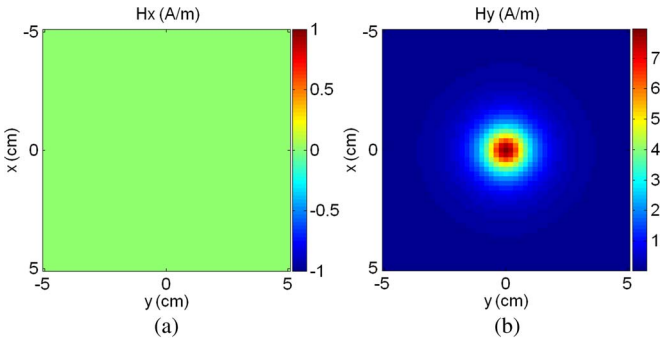

Fig. 6. Variations of the tangential magnetic field on a near-field plane ($h_1 = 10$ mm) produced by a small electrical dipole of length $l = 10$ mm at the center of the PCB plane (Fig. 1) when excited with a 1-A sinusoidal current source of frequency $f = 30$ MHz. (a) H_x and (b) H_y.

B. Small Electrical Dipole

In the next case study, we examine the performance of the proposed model when dealing with high-impedance sources. The radiating source is an electrical dipole of length $l = 10$ mm placed at the center of the PCB (Fig. 1). The dipole is excited with a 1-A sinusoidal current source at frequency $f = 30$ MHz.

We first obtain the simulated measured data on a near-field plane ($h_1 = 10$ mm) using the well-known field expressions for a radiating dipole in free space [18]. Results are shown in Fig. 6 for $SNR = 30$ dB. We then use the proposed model to obtain the equivalent current source on the PCB plane, as shown in Fig. 7. The equivalent current source is finally used to compute the magnetic-field distribution on a far-field plane ($h_2 = 50$ mm and $c = d = 400$ mm; Fig. 8). A quantitative comparison of the results (Table IV) confirms that the proposed model is capable of accurately reconstructing magnetic-field distributions at far-field regions for high-impedance sources.

C. DC–DC Converter

To further examine the validity of the proposed model, we analyze the experimental data obtained from the high-frequency section (dc–dc converter) of a typical SMPS. Fig. 9(a) shows a picture of the PCB containing the boost dc–dc converter used in the experiments. With reference to Fig. 9(b), the main components of the converter include a high-frequency inductor

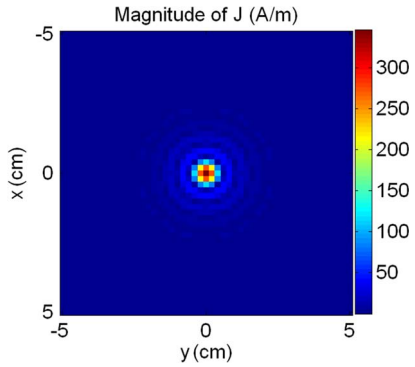

Fig. 7. Variations of the predicted current $(J_{\rm eq})$ on the PCB plane (Fig. 1) using the magnetic-field data shown in Fig. 6.

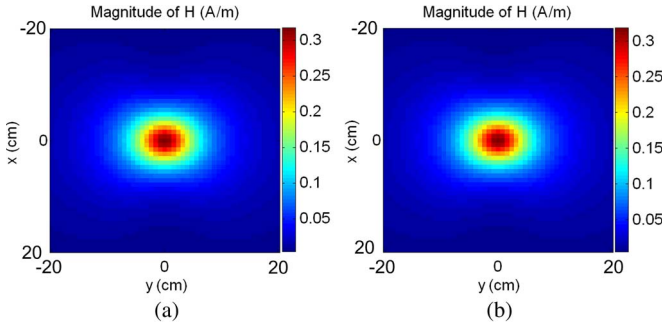

Fig. 8. Variations of the magnitude of magnetic field on a far-field plane $(h_2 = 50$ mm) produced by a small electrical dipole of length $l = 10$ mm at the center of the PCB plane (Fig. 1) when excited with a 1-A sinusoidal current source of frequency $f = 30$ MHz. (a) Theoretical and (b) reconstructed data.

TABLE IV
VALUES OF ADM, FDM, GDM, AND GRADE–SPREAD FOR ACTUAL AND RECONSTRUCTED RESULTS SHOWN IN FIG. 8

	ADM	FDM	GDM
	Excellent (0.0002)	Excellent (0.0001)	Excellent (0.0002)
Grade/Spread	1/1	1/1	1/1

$(L = 80$ mH), a high-frequency MOSFET switch (S) with heatsink, a rectifying diode D with heatsink, a resistive load $(R_L = 25\ \Omega)$, and low-frequency input $(C_i = 100\ \mu$F) and output $(C_o = 100\ \mu$F) capacitors. The circuit is fed by a dc power supply (15 V) via a connecting wire. The converter operates in continuous mode, giving an output dc voltage of 30 V. In order to amplify the radiated emissions, mitigation elements such as input EMI filters and Faraday shield are not included in the circuit [26], [27].

With a switching frequency of 100 kHz, various sections of the board [Fig. 9(b)] can radiate, including the input loop, high-frequency inductor, and heat sinks. This is inferred from the measured time-domain waveforms of the input loop current and MOSFET drain–source voltage, as shown in Fig. 10(a) and (b), respectively. The frequency spectrum of the current waveform can be divided in two sections. The first section constitutes low-frequency components, including the switching frequency and its harmonics. The second section includes high-frequency components such as the resonance frequencies corresponding

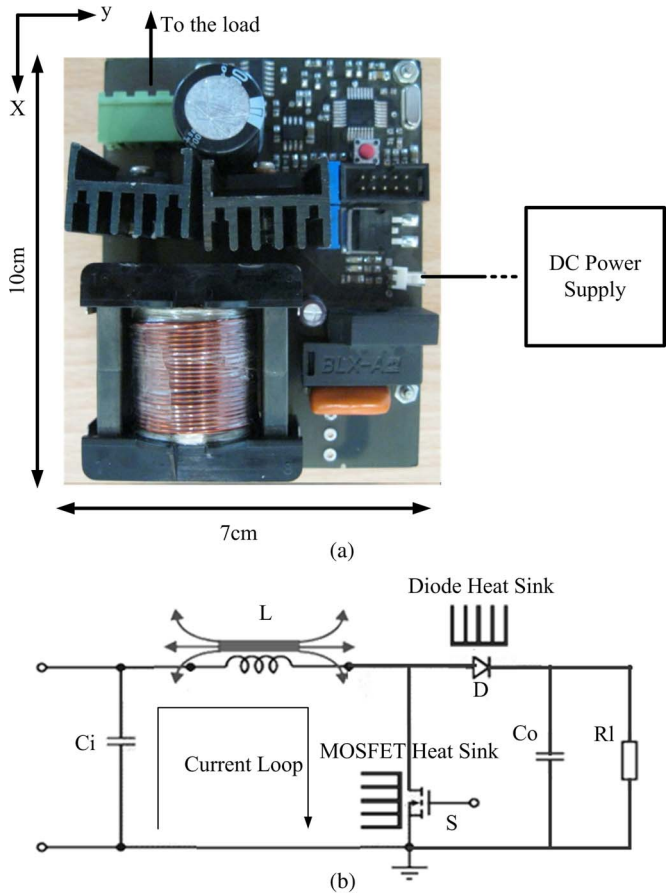

Fig. 9. (a) Photograph of the boost dc–dc converter used in the experiments and (b) the circuit diagram.

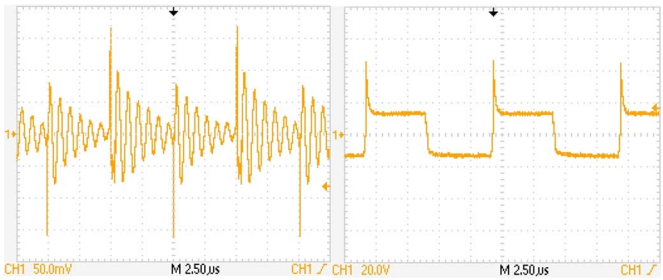

Fig. 10. Time-domain waveforms of (a) the input loop current and (b) MOSFET drain–source voltage in Fig. 9(b) measured by a 100-MHz Tektronix oscilloscope.

to the resonance between the intrinsic capacitances of the semiconductors and the parasitic inductances of the switching cell. The results shown in Fig. 11 illustrate the variations of the measured tangential magnetic field on a near-field plane $(h_1 = 10$ mm) corresponding to the one of the resonance frequencies at frequency $f = 16.8$ MHz for which the magnetic field attains its maximum value. Using the measured data, the proposed method is used to obtain the equivalent current source on the PCB plane, as shown in Fig. 12. A study of the results in this figure indicates that the current density concentrates on the locations of the inductor and the wire connection between the input dc power source and the PCB, demonstrating the validity of the proposed model. The equivalent current source is then

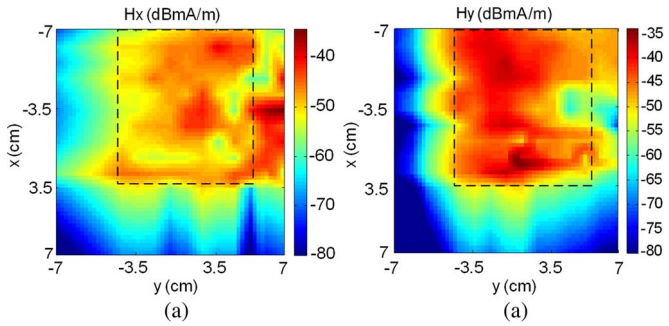

Fig. 11. Variations of the measured tangential magnetic field at $f = 16.8$ MHz produced by the dc–dc converter (Fig. 9) on the near-field plane ($h_1 = 10$ mm). (a) H_x and (b) H_y. Dotted line specifies the boundary of the PCB at $h = 0$.

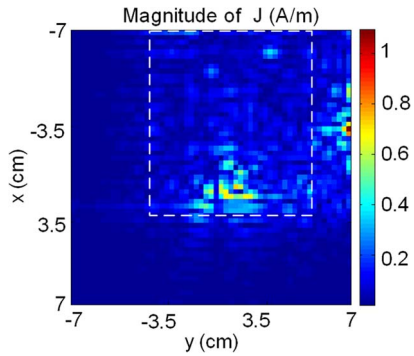

Fig. 12. Variations of the equivalent current ($J_{\rm eq}$) on the PCB plane ($z = 0$) predicted by the proposed model using the data shown in Fig. 11. Dotted line specifies the boundary of the PCB at $z = 0$.

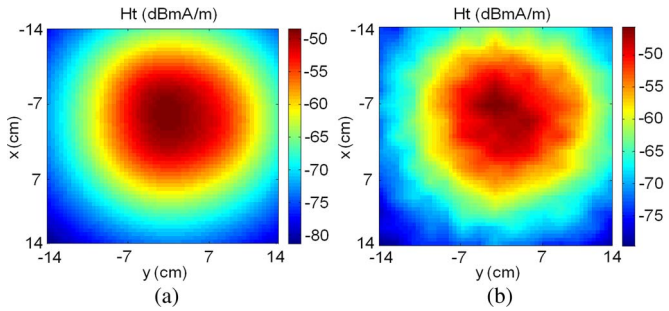

Fig. 13. Variations of the magnitude of magnetic field at $f = 16.8$ MHz produced by the dc–dc converter on a far-field plane ($h_2 = 50$ mm). (a) Reconstructed and (b) measured data.

used to reconstruct the tangential magnetic-field distribution on a far-field plane ($h_2 = 50$ mm), as shown in Fig. 13(a). The outcome of the FSV test for comparing the reconstructed and measured data (Fig. 13) is presented in Table V. The test data demonstrates that there is a good agreement between the theory and experiment. The existing differences are believed to be due to the finite size of the sampling surface size/mesh density among other inevitable uncertainties in the measurement process.

IV. Conclusion

A modeling technique, based on the electromagnetic equivalence principle, has been proposed to determine the radiated magnetic field from SMPSs on a typical PCB. The proposed technique first utilizes the tangential magnetic field measured on a given rectangular plane in the vicinity of the board to identify the radiating current sources on the PCB using the method-of-moments. Having determined the radiating sources, the magnetic-field distribution at a desired distance from the PCB is then computed using the governing integral equations in free space. The main feature of the proposed technique is its direct approach for the reconstruction of the radiating current sources which makes it much faster than the conventional techniques involving heuristic optimization algorithms. It is shown that the proposed technique is readily converged for a wide range of sampling distances on the field measurement plane. However, the number of measurement data should be large enough to achieve accurate results. Theoretical results supported by experiments have confirmed the accuracy of the proposed modeling technique.

TABLE V
Values of ADM, FDM, GDM, and Grade–Spread for Measured and Reconstructed Results Shown in Fig. 13

	ADM	FDM	GDM
Value	Good (0.288)	Good (0.300)	Fair (0.458)
Grade/Spread	4/4	4/4	4/3

References

[1] G. M. Dousoky, M. Shoyama, and T. Ninomiya, "FPGA based spread spectrum schemes for conducted-noise mitigation in dc–dc power converters: Design, implementation, and experimental investigation," *IEEE Trans. Ind. Electron.*, vol. 58, no. 2, pp. 429–435, Feb. 2011.

[2] L. A. BarragÃin, D. Navarro, J. Acero, I. Urriza, and J. M. BurdÃo, "FPGA implementation of a switching frequency modulation circuit for EMI reduction in resonant inverters for induction heating appliances," *IEEE Trans. Ind. Electron.*, vol. 55, no. 1, pp. 11–20, Jan. 2008.

[3] S. Kaboli, J. Mahdavi, and A. Agah, "Application of random PWM technique for reducing the conducted electromagnetic emissions in active filters," *IEEE Trans. Ind. Electron.*, vol. 54, no. 4, pp. 2333–2343, Aug. 2007.

[4] N. Mutoh, J. Nakashima, and M. Kanesaki, "Multilayer power printed structures suitable for controlling EMI noises generated in power converters," *IEEE Trans. Ind. Electron.*, vol. 50, no. 6, pp. 1085–1094, Dec. 2003.

[5] G. Antonini, S. Cristina, and A. Orlandi, "EMC characterization of SMPS device circuit and radiated emission model," *IEEE Trans. Electromagn. Compat.*, vol. 38, no. 3, pp. 300–309, Aug. 1996.

[6] A. M. Sitzia, A. E. Baker, T. W. Preston, A. Puzo, and A. Pons, "Finite element analysis for power electronics EMC applications," *IEEE Trans. Magn.*, vol. 32, no. 3, pp. 1517–1520, May 1996.

[7] N. J. Ryan, B. Chambers, and D. A. Stone, "FDTD modeling of heatsink RF characteristics for EMC mitigation," *IEEE Trans. Electromagn. Compat.*, vol. 44, no. 3, pp. 458–465, Aug. 2002.

[8] M. M. Hernando, A. Fernandez, M. Arias, M. Rodriguez, Y. Alvarez, and F. Las-Heras, "EMI radiated noise measurement system using the source reconstruction technique," *IEEE Trans. Ind. Electron.*, vol. 55, no. 9, pp. 3258–3265, Sep. 2008.

[9] M. Rodríguez, M. M. Hernando, M. Arias, Y. Álvarez, and F. Las-Heras, "Application of source reconstruction techniques and NF-FF transformations to estimate the EMI regulation compliance of a power electronic circuit," in *Proc. 23rd Annu. IEEE Appl. Power Electron. Conf. Expo.*, 2008, pp. 1741–1746.

[10] L. Beghou, B. Liu, L. Pichon, and F. Costa, "Synthesis of equivalent 3-D models from near field measurements—Application to the EMC of power printed circuit boards," *IEEE Trans. Magn.*, vol. 45, no. 3, pp. 1650–1653, Mar. 2009.

[11] O. Aouine, C. Labarre, and F. Costa, "Measurement and modeling of the magnetic near field radiated by a buck chopper," *IEEE Trans. Electromagn. Compat.*, vol. 50, no. 2, pp. 445–449, May 2008.
[12] T. K. Sarkar and A. Taaghol, "Near-field to near/far-field transformation for arbitrary near-field geometry utilizing an equivalent electric current and MoM," *IEEE Trans. Antennas Propagat.*, vol. 47, no. 3, pp. 566–573, Mar. 1999.
[13] F. Las-Heras and T. K. Sarkar, "A direct optimization approach for source reconstruction and NF-FF transformation using amplitude-only data," *IEEE Trans. Antennas Propagat.*, vol. 50, no. 4, pp. 500–510, Apr. 2002.
[14] F. Las-Heras, M. Rodríguez, S. Loredo, Y. Alvarez, and T. K. Sarkar, "Evaluating near-field radiation patterns of commercial antennas," *IEEE Trans. Antennas Propag.*, vol. 54, no. 8, pp. 2198–2207, Aug. 2006.
[15] Y. Álvarez, F. Las-Heras, and M. Rodríguez, "Reconstruction of equivalent currents distribution over arbitrary three-dimensional surfaces based on integral equation algorithms," *IEEE Trans. Antennas Propagat.*, vol. 55, no. 12, pp. 3460–3468, Dec. 2007.
[16] M. Rodríguez and T. K. Sarkar, "An improved super-resolution source reconstruction method," *IEEE Trans. Instrum. Meas.*, vol. 58, no. 11, pp. 3855–3866, Nov. 2009.
[17] R. F. Harrington, *Time-Harmonic Electromagnetic Fields*. New York, NY, USA: McGraw-Hill, 1961.
[18] A. Balanis, *Antenna Theory: Analysis and Design*. Hoboken, NJ, USA: Wiley, 2005.
[19] R. F. Harrington, *Field Computation by Moment Methods*. New York, NY, USA: Macmillan, 1968.
[20] C. C. Paige and M. A. Saunders, "LSQR: An algorithm for sparse linear equations and sparse least squares," *ACM Trans. Math. Soft.*, vol. 8, no. 1, pp. 43–71, Mar. 1982.
[21] K. Srinivasan, H. Sasaki, M. Swaminathan, and R. Tummala, "Calibration of near field measurements using microstrip line for noise predictions," in *Proc. IEEE Electron. Compon. Technol. Conf.*, Jun. 2004, vol. 2, pp. 1432–1436.
[22] X. Tong, D. W. P. Thomas, A. Nothofer, P. Sewell, and C. Christopoulos, "Modeling electromagnetic emissions from printed circuit boards in closed environments using equivalent dipoles," *IEEE Trans. Electromagn. Compat.*, vol. 52, no. 2, pp. 462–470, May 2010.
[23] A. P. Duffy, A. J. M. Martin, A. Orlandi, G. Antonini, T. M. Benson, and M. S. Woolfson, "Feature Selective Validation (FSV) for validation of computational electromagnetics (CEM). Part I—The FSV method," *IEEE Trans. Electromagn. Compat.*, vol. 48, no. 3, pp. 449–459, Aug. 2006.
[24] A. Orlandi, A. P. Duffy, B. Archambeault, G. Antonini, D. E. Coleby, and S. Connor, "Feature Selective Validation (FSV) for validation of computational electromagnetics (CEM). Part II—Assessment of FSV performance," *IEEE Trans. Electromagn. Compat.*, vol. 48, no. 3, pp. 460–467, Aug. 2006.
[25] *IEEE Standard for Validation of Computational Electromagnetics Computer Modeling and Simulation*, IEEE Std. P1597.1, 2008.
[26] K. Raggl, T. Nussbaumer, and J. Kolar, "Guideline for a simplified differential-mode EMI filter design," *IEEE Trans. Ind. Electron.*, vol. 57, no. 3, pp. 1031–1040, Mar. 2010.
[27] H.-I. Hsieh, J.-S. Li, and D. Chen, "Effects of X capacitors on EMI filter effectiveness," *IEEE Trans. Ind. Electron.*, vol. 55, no. 2, pp. 949–955, Feb. 2008.

Sayyed Mohammad Mehdi Mirtalaei received the B.S. degree in electrical engineering from Isfahan University of Technology, Isfahan, Iran, in 2005 and the M.S. and Ph.D. degrees in electrical engineering from Amirkabir University of Technology, Tehran, Iran, in 2007 and 2013, respectively.

He is with the Department of Electrical Engineering, Amirkabir University of Technology. His research interests are power electronics, electromagnetic interference/electromagnetic compatibility, and the numerical method in electromagnetics.

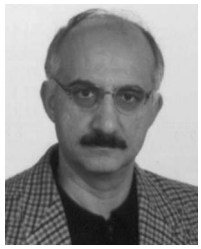

Seyed Hossein H. Sadeghi (M'92–SM'05) received the B.S. degree in electrical engineering from Sharif University of Technology, Tehran, Iran, in 1980, the M.S. degree in power engineering from the Institute of Science and Technology, University of Manchester, Manchester, U.K., in 1984, and the Ph.D. degree in electronic systems engineering from Essex University, Colchester, U.K., in 1991.

In 1992, he was appointed as a Research Assistant Professor with Vanderbilt University, Nashville, TN, USA. He is a Professor of electrical engineering with Amirkabir University of Technology, Tehran, Iran. He is the holder of three patents and the author or coauthor of one book and over 250 scientific papers published in reviewed journals and presented in international conferences. His current research interests include electromagnetic nondestructive evaluation of materials and electromagnetic compatibility issues in power engineering. He is currently a Visiting Professor at the University of Wisconsin, Milwaukee, WI, USA.

Ruzbeh Moini (A'89–M'93–SM'06) received the B.S, M.S., and Ph.D. degrees in electronics from Limoges University, Limoges, France, in 1984, 1985, and 1988, respectively.

In 1988, he joined Amirkabir University of Technology, Tehran, Iran, where he is a Professor of electrical engineering. He is the author or coauthor of one book and more than 200 scientific publications in reviewed journals and international conferences. His current research interests include numerical methods in electromagnetics, electromagnetic compatibility, and antenna theory. He is currently a Visiting Professor with the University of Toronto, Toronto, ON, Canada.